The Journal of Physiology

Increased circulating microparticles in streptozotocin-induced diabetes propagate inflammation contributing to microvascular dysfunction

Qilong Feng[1,2,7], Christian J. Stork[2], Sulei Xu[1,2], Dong Yuan[2], Xinghai Xia[1], Kyle B. LaPenna[1], Ge Guo[2], Haoyu Sun[1], Li-Chong Xu[3], Christopher A. Siedlecki[3], Kathleen M. Brundage[4], Nate Sheaffer[5], Todd D. Schell[5,6] and Pingnian He[1,2]

[1] *Department of Cellular and Molecular Physiology, College of Medicine, Penn State University, Hershey, PA 17033, USA*
[2] *Department of Physiology and Pharmacology, School of Medicine, West Virginia University, Morgantown, WV 26506, USA*
[3] *Department of Surgery, College of Medicine, Penn State University, Hershey, PA 17033, USA*
[4] *Department of Microbiology, Immunology and Cell Biology, School of Medicine, West Virginia University, Morgantown, WV 26506, USA*
[5] *Flow Cytometry Core, College of Medicine, Penn State University, Hershey, PA 17033, USA*
[6] *Department of Microbiology and Immunology, College of Medicine, Penn State University, Hershey, PA 17033, USA*
[7] *Department of Physiology, Shanxi Medical University, Taiyuan, Shanxi, China 030001*

Edited by: Kim Barrett & Javier Gonzalez

Key points

- Circulating microparticles (MPs) are elevated in many cardiovascular diseases and have been considered as biomarkers of disease prognosis; however, current knowledge of MP functions has been mainly derived from *in vitro* studies and their precise impact on vascular inflammation and disease progression remains obscure.
- Using a diabetic rat model, we identified a >130-fold increase in MPs in plasma of diabetic rats compared to normal rats, the majority of which circulated as aggregates, expressing multiple cell markers and largely externalized phosphatidylserine; vascular images illustrate MP biogenesis and their manifestations in microvessels of diabetic rats.
- Using combined single microvessel perfusion and systemic cross-transfusion approaches, we delineated how diabetic MPs propagate inflammation in the vasculature and transform normal microvessels into an inflammatory phenotype observed in the microvessels of diabetic rats.
- Our observations derived from animal studies resembling conditions in diabetic patients, providing a mechanistic insight into MP-mediated pathogenesis of diabetes-associated multi-organ microvascular dysfunction.

Abstract In various cardiovascular diseases, microparticles (MPs), the membrane-derived vesicles released during cell activation, are markedly increased in the circulation. These MPs have been recognized to play diverse roles in the regulation of cellular functions. However, current

Qilong Feng has worked on microparticles (MPs) since 2014 as a postdoctoral fellow at the College of Medicine, Penn State University. It was quite a challenge to characterize the plasma microparticles using flow cytometry due to their sub-micron sizes. Inspiringly, he and his teammates overcame many technical issues and provided experimental evidence that diabetic MPs actively disseminate inflammation in the vasculature, contributing to diabetes-associated microvascular dysfunction. Dr Feng now is a professor in the Department of Physiology, Shanxi Medical University, China. He plans to further investigate the roles of circulating microparticles in cardiac ischaemia models.

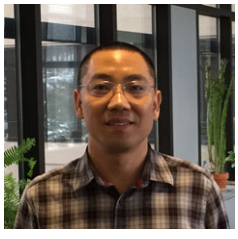

DOI: 10.1113/JP277312

knowledge of MP function has been largely derived from *in vitro* studies. The precise impact of disease-induced MPs on vascular inflammation and disease progression remains obscure. In this study we investigated the biogenesis, profile and functional roles of circulating MPs using a streptozotocin-induced diabetic rat model with well-characterized microvascular functions. Our study revealed a >130-fold increase in MPs in the plasma of diabetic rats compared to normal rats. The majority of these MPs originate from platelets, leukocytes and endothelial cells (ECs), and circulate as aggregates. Diabetic MPs show greater externalized phosphatidylserine (PS) than normal MPs. When diabetic plasma or isolated diabetic MPs were perfused into normal microvessels or systemically transfused into normal rats, MPs immediately adhered to endothelium and subsequently mediated leukocyte adhesion. These microvessels then exhibited augmented permeability responses to inflammatory mediators, replicating the microvascular manifestations observed in diabetic rats. These effects were abrogated when MPs were removed from diabetic plasma or when diabetic MPs were pre-coated with a lipid-binding protein, annexin V, suggesting externalized PS to be key in mediating MP interactions with endothelium and leukocytes. Our study demonstrated that the elevated MPs in diabetic plasma are actively involved in the propagation of vascular inflammation through their adhesive surfaces, providing mechanistic insight into the pathogenesis of multi-organ vascular dysfunction that commonly occurs in diabetic patients.

(Received 13 October 2018; accepted after revision 11 December 2018; first published online 11 December 2018)
Corresponding author P. He: Department of Cellular and Molecular Physiology, College of Medicine, Penn State University, Hershey, PA 17033, USA. Email: pinghe@hmc.psu.edu

Introduction

Increasing clinical evidence indicates that circulating microparticles (MPs) are markedly elevated in patients with inflammation-linked cardiovascular diseases, including diabetes (Agouni *et al.* 2008; Leroyer *et al.* 2008*a*; Jung *et al.* 2009; Boilard *et al.* 2010; Helal *et al.* 2010; Meziani *et al.* 2010; Tramontano *et al.* 2010; Mastronardi *et al.* 2011; Berezin & Kremzer, 2015; Berezin *et al.* 2015; Pasquier *et al.* 2017). MPs, the small plasma membrane-derived vesicles released during cell activation and apoptosis, often retain membrane surface molecules, cytoplasmic proteins, lipids and nucleic acids from their parent cells, and have been recognized as important biomarkers of disease status. While increasing numbers of studies have focused on the potential roles of circulating MPs as diagnostic tools (Berezin *et al.* 2015; La Marca & Fierabracci, 2017; Michalska-Jakubus *et al.* 2017; Pasquier *et al.* 2017; Ridger *et al.* 2017; Hosseinzadeh *et al.* 2018), their precise impact on the pathogenesis and progression of diseases remains obscure (Nomura *et al.* 2008). Currently, functional MP studies have been conducted mainly on specific cell type-derived MPs using *in vitro* approaches (Leroyer *et al.* 2008; Badimon *et al.* 2017; Burger *et al.* 2017). There has been a lack of *in vivo* evidence demonstrating the characteristics of circulating MPs produced under disease conditions and their functional roles in vascular dysfunction and disease progression (Puddu *et al.* 2010; Yun *et al.* 2016).

In this study we investigated the biogenesis, profile and functional roles of circulating MPs in diabetes-associated microvascular dysfunction using a diabetic rat model in which the microvessel permeability properties have been previously well characterized. Our studies had demonstrated that microvessels of streptozotocin (STZ)-induced diabetic rats exhibit an inflammatory phenotype with increased baseline permeability, increased leukocyte adhesion, and a markedly potentiated permeability response to inflammatory mediators (Yuan *et al.* 2014). These observations resembled the exaggerated inflammation that commonly occurs in diabetic patients with an acute infection. To characterize the plasma MPs and identify their roles in the development of the inflammatory phenotype observed in microvessels of diabetic rats, we combined flow cytometry analysis of MPs with single vessel perfusion, systemic cross-animal plasma transfusion, confocal imaging, electron microscopy, and quantitative permeability measurements in intact microvessels. The single vessel perfusion approach enabled us to illustrate MP-mediated pathological processes in intact microvessels, and thus to reveal how diabetes-induced MPs propagate inflammation in the vasculature and transform normal microvessels into an inflammatory phenotype observed in the microvessels of diabetic rats.

Methods

Ethical approval

All procedures and animal use were approved by the Animal Care and Use Committee at West Virginia University (12-0707) or the College of Medicine at

Pennsylvania State University (46306). The Animal Resource Programs at both Institutions are accredited by the American Association for the Accreditation of Laboratory Animal Care (AALAC), and meet National Institutes of Health standards as set forth in the *Guide for the Care and Use of Laboratory Animals*, and conform to the principles and regulations as described in *The Journal of Physiology* editorial by Grundy (2015). All animals were purchased from Institution Animal Care and Use Committee-approved venders and kept in an AALAC-approved animal facility with *ad libitum* access to food and water. STZ-induced diabetic rats were monitored daily. If the animal lost more than 20% of body weight and/or exhibited a drop in body condition score to 1 or 2, a timely intervention, removal from the study, or humane killing (overdose of sodium pentobarbital by intraperitoneal injection 200 mg/kg body wt) was performed.

Animal preparation

All animal experiments were conducted on Sprague-Dawley rats (2–3 months old, 220–250 g; Hilltop Laboratory Animal, Scottdale, PA, USA or Sage Laboratory, Boyertown, PA, USA) following approved procedures. All results were derived from female rats except the data presented in Fig. 3, which included 8 age-matched male rats. Diabetic rats were induced by a single intraperitoneal injection of STZ in citrate buffer (60 mg/kg body weight) after fasting for 8 h. Increased blood glucose was detected 24–48 h after the STZ injection. Experiments were conducted in rats that experienced hyperglycaemia (>350 mg/ml) for 2–3 weeks. The average fasting blood glucose level of normal rats was 102 ± 4 mg/dl ($N = 8$) and STZ-injected rats ($N = 20$) was 448 ± 10 mg/dl, and the haemoglobin A1c of STZ rats measured before the experiments was 88 ± 1.5 (mmol HbA1c/mol Hb). The measurements of serum creatinine and blood urea nitrogen were performed by the Department of Comparative Medicine at Penn State University using the Cobas Mira Plus Chemistry Analyzer.

Blood collection was performed through carotid cannulation in rats under anaesthesia with intraperitoneal-administration of sodium pentobarbital (65 mg/kg body wt), and sodium citrate (3.8%, 9:1 ratio, v/v) was used as anticoagulant. Individual vessel perfusion experiments were conducted in the mesentery of rats (He *et al.* 1996; Jiang *et al.* 2008) under anaesthesia through subcutaneous administration of inactin hydrate. The initial dosage of inactin was 170 mg/kg body wt and an additional 20 mg/dose was given as needed. To avoid or minimize pain or distress to animals, the anaesthesia status was evaluated and monitored before and during the experiment by checking responses of spinal reflexes to stimuli. The loss of toe pinch reflex is served as an indicator of the appropriate plane of anesthesia.

To prepare rats for single vessel perfusion experiments, a midline surgical incision (1.5–2 cm) was made in the abdominal wall and the mesentery was gently moved out from the abdominal cavity and spread over a pillar or a glass coverslip attached to an animal tray for hydraulic conductivity (L_p) measurements or confocal imaging in individually perfused microvessels. The upper surface of the mesentery was continuously superfused with mammalian Ringer solution at 37°C, and the animal was kept warm via heating pad placed underneath the surgical tray. Each experiment was performed on one microvessel per animal to avoid any potential effect of the applied reagents on subsequent vessel studies.

After exsanguination, or the single vessel perfusion experiment, the animal was killed by performing a bilateral thoracotomy while under general anesthesia with confirmed anesthesia status, a method consistent with the recommendations of the American Veterinary Medical Association (AVMA) Guidelines for the Euthanasia of Animals (2013 edition).

Flow cytometry analysis of plasma and isolated MPs

A BD LSR Fortessa cytometer (BD Biosciences San Jose, CA, USA) was used for MP analysis. All reagents and buffers were sterile filtered using a 0.1 μm PVDF filter (Millex-VV, Darmstadt, Germany). Freshly collected blood samples were centrifuged at 1550 *g* for 20 min at 20°C to obtain platelet-free plasma (PFP), and the aliquots were immediately frozen at −80°C. For the flow cytometry analysis of plasma MPs, aliquots of PFP were thawed at room temperature and each sample was split into two tubes for duplicate measurements. Each PFP sample was first diluted with Dulbecco's phosphate-buffered saline (PBS, MP Biomedicals) at ratios of 1:100 to 1:1000 (based on the estimated amount of MPs in the sample) for counting. MPs were size-gated using 220, 450, 880 and 1330 nm calibration beads (Spherotech Inc., USA), and the total events were calculated by subtracting the background of buffer alone in the gate. To quantify the number of MPs per volume, a known number of 5.0 μm diameter counting beads (Duke Scientific Corp; Palo Alto, CA, USA) were included in some samples of the experiment and the bead concentration was counted manually via a haemocytometer. In addition, the volume collected by the instrument was calibrated daily by running water for 5 min at the same flow rate as the samples (low rate) and calculating the volume difference in the tube before and after sample acquisition. MPs were expressed as MPs per microlitre (μl) of plasma. To maintain a similar range of events in each assay and a consistent fluorescent marker-to-MP ratio for annexin V (AnnV) and antibody binding, PFP was pre-diluted (depending on the MP concentration of the sample) to give total events about 50,000/min at flow rate 20 μl/min for flow analysis, and

the MP concentration in the initial binding solution (total volume of 100 μl) was about 10,000/μl. For AnnV staining, heparin was added to each PFP sample at 40 units/ml before adding fluorochrome conjugated AnnV (3 μl) and AnnV binding buffer (10 mM $CaCl_2$, 140 mM NaCl, and 10 mM HEPES at pH 7.4). We found that the use of 10 mM, instead of 2.5 mM $CaCl_2$, in the solution for initial incubation increases the MP binding to AnnV, which is consistent with other reports, especially for MPs with larger PS exposed surface area (Tait & Gibson, 1992). After 20 min incubation in the dark at room temperature, the sample in the binding solution (100 μl) was further diluted with 300 μl AnnV binding buffer containing 3 mM $CaCl_2$ to give a final calcium concentration of 5 mM for AnnV analysis. For multiple antibody staining, 5 μl each of pre-diluted specific anti-CD61, anti-CD144, and anti-CD45 fluorescent conjugated monoclonal antibodies (to concentrations found to be optimal in preliminary experiments) were added to samples diluted with PBS before incubation. To identify the cell origins of aggregated MPs, double positively stained MPs were shown as either CD45+/CD61+, CD45+/CD144+, or CD61+/CD144+. For triple-stained MPs, shown as CD45+/CD61+/CD144+, we first selected one of the double positive quadrants and then gated using the third antibody.

The specificity of antibodies CD45-PE and CD61-APC were validated by labelling white blood cells and platelets, the MP parental cells, isolated from rat plasma, respectively. Since isotype controls may generate false negative or positive MPs in flow cytometry (Trummer *et al.* 2008; Dey-Hazra *et al.* 2010), we used fluorescence minus one (FMO) (Orozco & Lewis, 2010; van Ierssel *et al.* 2010) controls to discriminate true events from noise and to increase the specificity for MP detection. Negative controls for antibody aggregates were prepared in buffer with all the antibodies present but no MPs. Negative controls for AnnV were prepared in buffer lacking $CaCl_2$. The gated cell membrane-derived MP population was further confirmed by TEM images after Triton X-100 (0.5%) lysis. Data analysis was performed using FCS Express software (De Novo Software). MP-free plasma was achieved via centrifugation and filtration (0.1 μm filter) and confirmed by flow cytometry.

Measurement of L_p in individually perfused rat mesenteric microvessels

Microvessel permeability was assessed by measuring hydraulic conductivity, L_p, using a modified Landis technique (He *et al.* 2006). An individual mesenteric venule was cannulated with a micropipette and perfused with albumin-Ringer solution (control) containing red blood cells (~1% v/v) as a marker under a known hydrostatic pressure (40–60 cmH_2O) with intact surrounding circulation. For each measurement, the perfused vessel was occluded briefly downstream with a glass rod. The initial water flux/unit area of microvessel wall (J_v/A) was calculated from the velocity of the marker cell after vessel occlusion, the vessel radius, and the distance between the marker cell and the occlusion site. L_p was calculated as the slope of the relationship between J_v/A and the pressure difference across the vessel wall. Each L_p value presented in the results and figures is the mean of a series of measurements (5-15) under one condition in a certain time period. In each experiment, the mean baseline L_p and the L_p after the application of testing solutions were measured in the same vessel. To measure L_p and leukocyte adhesion in PFP-perfused microvessels, PFP prepared from citrated blood (3.8% w/v) was heparinized (40 units/ml) and re-calcified using 100 mM $CaCl_2$ to a concentration of 18 mM to achieve a physiological calcium concentration in plasma (Ramstrom, 2005). The re-calcified PFP was mixed with Ringer solution (1:1, v/v) before perfusing vessels. The protein content of each solution was measured with refractometer. In each experiment, the baseline L_p was measured first using BSA (2%)-Ringer solution. The same vessel was then perfused with 50% PFP for 30 min followed by resumed blood flow for 10 min to allow the endogenous blood cells to interact with endothelial cells (ECs) that had been exposed to perfused PFP. The changes in L_p were measured when the vessel was perfused with either normal or diabetic PFP before and after resumed blood flow. The leukocytes adhering to the microvessel wall were counted and expressed as the number of adherent leukocytes per 100 μm microvessel length before and after PFP perfusion. Figure 6*B* shows schematic procedures.

Confocal imaging

Confocal images were acquired from a Leica TCS SL confocal system equipped with a single microvessel perfusion rig. A Leica ×25 objective (HCX IRAPO, NA 0.95) was used for image acquisition. Images were collected using one airy pinhole diameter, 1024 × 1024 pixels scanning format, and 0.5 μm vertical steps (z-axis). Each venule at rat mesentery was perfused with normal or diabetic PFP or a solution containing equal numbers of isolated MPs from either diabetic or normal rat plasma for 30 min followed by 10 min perfusion of albumin-Ringer solution containing 1:20 AnnV Alexa-488 to label adherent MPs. Images were acquired after removal of unbound AnnV from the vessel lumen by albumin-Ringer perfusion. In some experiments, after MP perfusion, blood flow was resumed for 10 min to allow leukocytes to interact with adherent MPs, and Alexa-647 conjugated anti-CD45 was perfused along with AnnV to label both MPs and adherent leukocytes. An Argon laser (488 nm) and a HeNe laser (633 nm) were used for excitation of Alexa-488

and Alexa-647 with emissions between 530–560 nm and 650–690 nm, respectively. Identical image acquisition parameters were applied to each group of experiments. Stacks of images were processed using Leica confocal software. Isolated MPs were prepared from PFP of normal and diabetic rats by ultracentrifugation at 20,200 *g* for 45 min at 20°C to collect the MP pellet followed by a PBS wash and another ultracentrifugation with the same settings. Freshly isolated MPs were diluted to a final concentration of 8600 AnnV+ MPs/μl in albumin-Ringer solution for perfusion experiments. Stacks of images were obtained from the lower half of each vessel by optical sectioning at successive *x-y* focal planes through the *z*-axis. Stimulated emission depletion (STED) microscopy was used to detect aggregated plasma MPs with multiple cell markers. Anti-CD45-PE (Biolegend), anti-CD61-APC (Biolegend) and bodipy FL Dye (Thermo Fisher Scientific) were used to identify leukocyte and platelet derived MPs, and their interaction with lipid droplets. Images were obtained using a ×100 oil immersion objective with a 1.4 numerical aperture. Laser excitation wavelengths of 488 nm, 633 nm, and 561 nm were used in addition to STED depletion laser wavelengths of 592 nm, 755 nm, and 775 nm, respectively. Images were obtained at a resolution of 38 nm by Leica hybrid detectors.

Electron microscopy

Transmission electron microscopy was performed to illustrate MPs in the plasma of diabetes rats. Plasma was fixed and pre-stained with 2% osmium (2:1 ratio, v/v) for 30 min and post stained with 2% phosphotungstic acid solution at pH 7.0 for 5 s on Rae coated copper grids. The images were acquired by a JEOL 1400 TEM with an Orius SC1000 CCD camera.

Atomic force microscopy

Samples for atomic force microscopy (AFM) were prepared from isolated MPs diluted in PBS to a concentration of $3 \times 10^4/\mu$l. The MP sample (50 μl) was placed onto a freshly peeled mica surface for 5 min, and slightly flushed with nitrogen to air dry the sample. After adsorption, the sample was carefully washed three times with distilled water to remove any traces of salts. The measurements were performed using a Multimode AFM with a Nanoscope IIIa control system (software version 5.31r1, Digital Instruments, Santa Barbara, CA, USA) operating in tapping mode, with AFM probes (Tetra, K-Tek Nanotechnology, Wilsonville, OR, USA) of nominal radius of curvature 10 nm, length 125 μm, spring constant 5.0 N/m, and resonant frequency of 160 kHz. The images were extracted and analysed with offline software NanoScope Analysis (Version 1.50 Bruker).

Materials

Mammalian Ringer solution was used for surgery procedures, mesentery preparation, superfusing tissue, and preparing the perfusion solutions. The composition of the mammalian Ringer solution was (in mM): 132 NaCl, 4.6 KCl, 2 $CaCl_2$, 1.2 $MgSO_4$, 5.5 glucose, 5 $NaHCO_3$, and 20 HEPES/Na-HEPES; pH was maintained at 7.40-7.45 by adjusting the ratio of Na-HEPES to HEPES. All perfusates used for control and test perfusion contained BSA (10–20 mg/ml). The composition of annexin V binding buffer was: 10 mM HEPES pH 7.4, 140 mM NaCl, and 10 or 3 mM $CaCl_2$. Reagents were purchased from Sigma-Aldrich (St Louis, MO, USA) unless indicated otherwise.

AnnV Alexa-488 was purchased from Invitrogen (Cat. No. A13201, Carlsbad, CA, USA). For multiple specific antibody staining, Anti-CD45-PE (Cat. No. 2022207, RRID:AB_314006, Biolegend), anti-CD61-APC (Cat. No.104314, RRID:AB_2234024, Biolegend) and anti-CD144-FITC (Cat. No. ALX-210-232F-T100, Enzo Life Sciences) were used.

Statistical analysis

All values are means ± SEM. A Student's paired *t* test (nonparametric Wilcoxon matched-pairs signed rank test, two-tailed) was used for paired experiments conducted in the same vessel, and a Mann-Whitney test (two-tailed) was used for data comparison between two groups. ANOVA with a Tukey *post hoc* test was used to compare data among multiple groups. A probability value of $P < 0.05$ was considered statistically significant. Each *N* value in the flow cytometry analysis represents the number of rats from which plasma was collected, and the mean of duplicate analyses in each sample, and each *N* value from the microvessel perfusion experiment represents one experiment conducted in each rat.

Results

Characterization of MPs in plasma of diabetic rats

The MPs in plasma of normal and diabetic rats were characterized with flow cytometry and visualized by STED microscopy, transmission electron microscopy, and atomic force microscopy. Figure 1 shows the results of flow cytometry analysis. The population of MPs was gated in the size range between 0.1 to 1 μm (Fig. 1*A* and *B*). MPs were markedly elevated in plasma of diabetic rats ($594.7 \pm 201.6 \times 10^4/\mu$l) compared to that in normal rats ($4.5 \pm 0.7 \times 10^4/\mu$l, $N = 8$ per group, $P = 0.0002$). MPs with phosphatidylserine (PS) exposure identified by positive binding to fluorescent labelled AnnV increased from $3.5 \pm 0.7 \times 10^4/\mu$l in normal rats to $521.3 \pm 170.8 \times 10^4/\mu$l in diabetic rats ($N = 8$ per group,

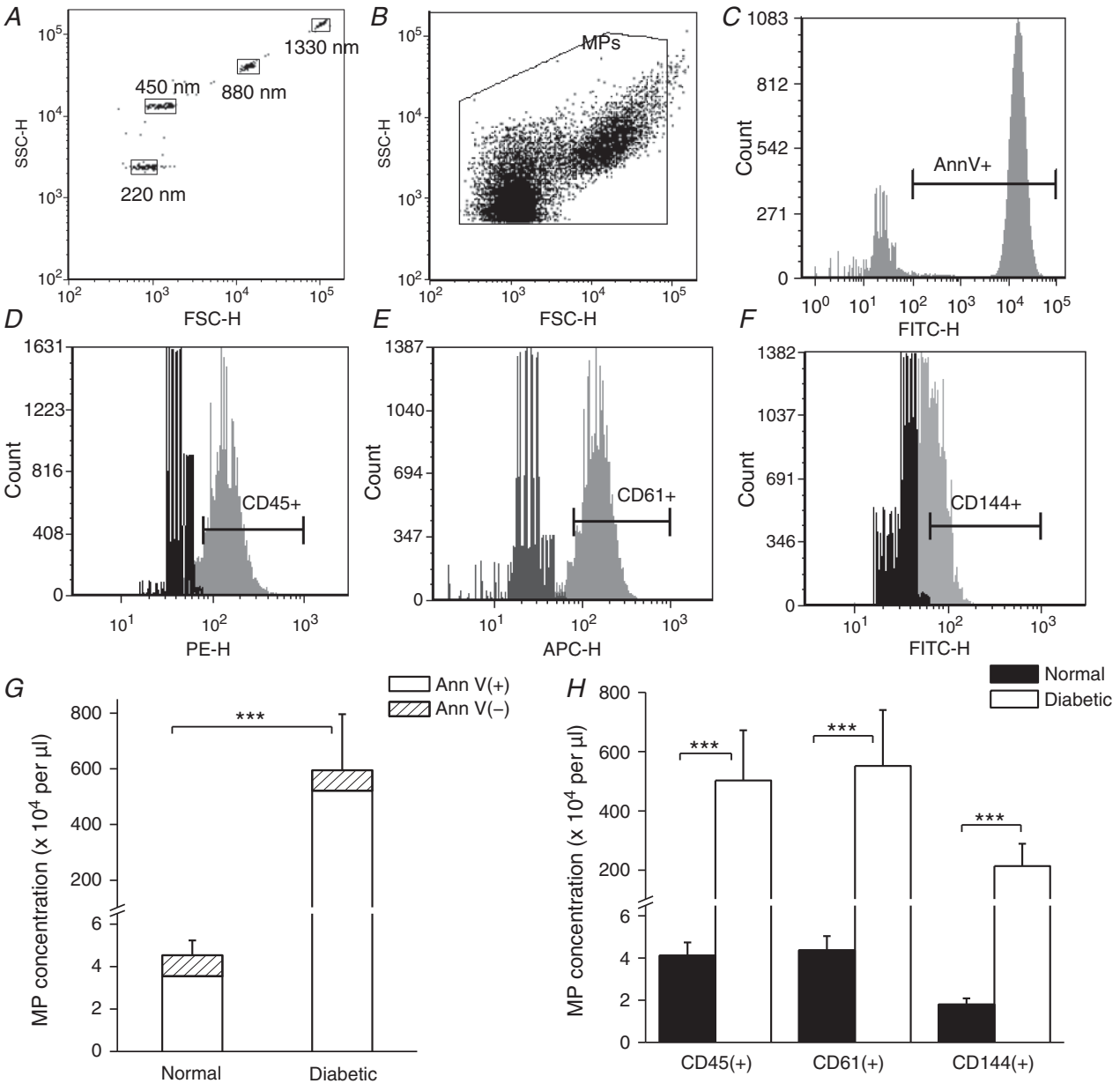

Figure 1. Flow cytometry analysis of microparticles (MPs) in rat plasma
A, polystyrene calibration beads with diameters of 220, 450, 880 and 1330 nm were used for forward scatter (FSC) and side scatter (SSC) calibration. *B*, representative dot plot of gated particles in normal rat plasma with forward scatter (FSC) on the *x*-axis (proportional to particle size) and side scatter (SSC) on the *y*-axis (proportional to the particle granularity); both axes are in log-scale. *C*, representative histogram showing FITC-conjugated annexin-V (AnnV) positive particles. The positive MP fluorescence intensity range is indicated by the horizontal bar. *D–F*, flow cytometry detection of MPs labelled with fluorescence-conjugated cell marker specific antibodies showing MPs originated from leukocytes (CD45+), platelets (CD61+) and endothelial cells (CD144+). Gates were set up using fluorescence minus one (FMO) controls (shown in black). *G*, summary graph of flow cytometry analyses for plasma MPs showing that the total number of MPs dominated by AnnV-positive (phosphatidylserine exposed) MPs was significantly increased in diabetic rats compared to normal rats. ($N = 8$ for each group, $^{***}P = 0.0002$). *H*, the cell origin characterization of MPs from the same samples shown in *G* demonstrates that the majority of the increased MPs in plasma of diabetic rats are derived from leukocytes, platelets and endothelial cells ($^{***}P \leq 0.001$, $N = 8$ per group).

$P = 0.0001$), contributing to 77.9% and 92.3% of the total MPs in normal and diabetic plasma, respectively. The MP cellular origins in those samples were differentiated using fluorescent conjugated antibodies directed against cell specific antigens. Leukocytes, platelets and endothelial cells were the main sources for total MPs. Figure 1*C–F* shows the representative fluorescent marker analyses, and panels *G* and *H* show the results summary. The antibody specificity was validated with specific cell staining from the same animal species and the gated MP population was confirmed by triton lysis (Orozco & Lewis, 2010; Gyorgy *et al.* 2011). Multi-channel flow cytometry analysis

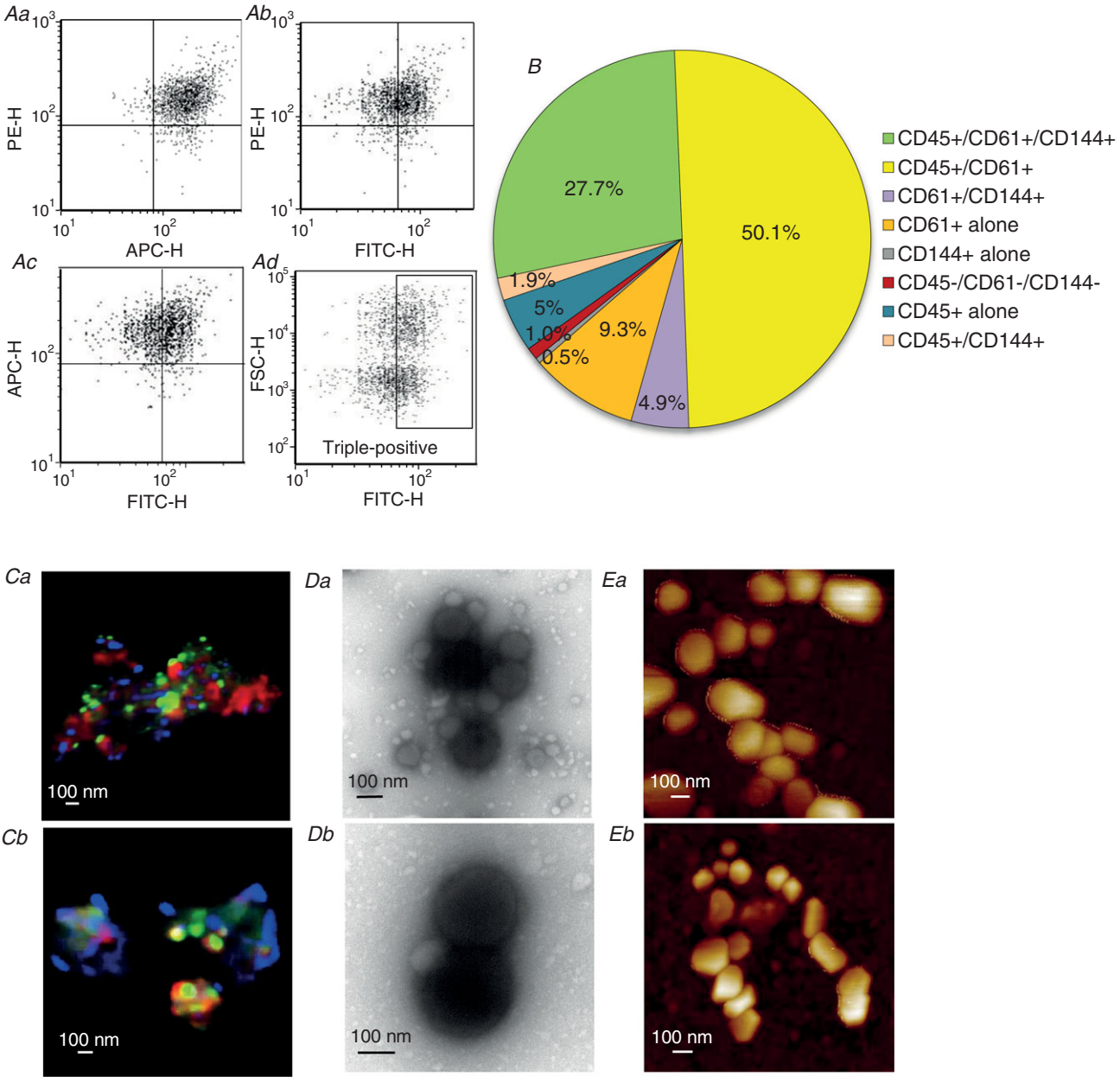

Figure 2. A majority of MPs express multiple cell markers indicating that MPs derived from different cell origins aggregate in the circulation
A and *B*, flow cytometry analysis of diabetic rat plasma showing that 85% of MPs express triple and double cell markers ($N = 8$). *C–E*, morphology studies of plasma MPs in diabetic rats using confocal microscopy (*Ca* and *b*), transmission electronic microscopy (TEM) (*Da* and *b*), and atomic force microscopy (AFM) (*Ea* and *b*). Confocal imaging demonstrated that the aggregated MPs are from different cellular sources, which were identified by antibodies directed against specific cell markers: platelets (CD61, red), leukocytes (CD45, blue). The MPs were also aggregated with lipid droplets (bodipy, green). TEM and AFM confirmed the aggregated form of MPs in the plasma. $N = 3$–4 per approach.

Table 1. Characterizations of MP levels (× 10^4 per μl) and cell origins in normal and diabetic rat plasma

Gates	Normal plasma	%	Diabetic plasma	%
Total MPs	4.53 ± 0.70		594.69 ± 201.60*	
AnnV positive	3.54 ± 0.70	77.90 ± 4.45	521.33 ± 170.82*	92.34 ± 3.22*
Triple positive				
CD45+/CD61+/CD144+	1.64 ± 0.28	36.33 ± 3.02	169.96 ± 59.47*	27.68 ± 2.18*
Double positive				
CD45+/CD61+	2.35 ± 0.38	52.07 ± 1.57	297.96 ± 100.92*	50.09 ± 2.06
CD61+/CD144+	0.12 ± 0.03	2.56 ± 0.27	30.59 ± 11.28*	4.93 ± 0.50*
CD45+/CD144+	0.03 ± 0.01	0.63 ± 0.13	10.86 ± 3.37*	1.93 ± 0.11*
Single positive				
Single CD45+	0.10 ± 0.03	2.22 ± 0.45	23.84 ± 6.92*	4.60 ± 0.65*
Single CD61+	0.26 ± 0.07	5.62 ± 0.81	53.22 ± 18.15*	9.26 ± 0.44*
Single CD144+	0.01 ± 0.003	0.15 ± 0.04	2.79 ± 1.02*	0.48 ± 0.05*
Negative				
CD45−/CD61−/CD144−	0.02 ± 0.01	0.46 ± 0.13	5.46 ± 2.08*	1.03 ± 0.16*

Results are derived from 8 normal and 8 diabetic rats and presented as means and standard errors. *$P < 0.05$ *vs.* normal.

revealed that the majority of the MPs existed as aggregated units expressing multiple cell surface antigens (Fig. 2*A*). About 30% of the MPs carried triple antigens (leukocyte: CD45; platelet: CD61; endothelial cell: CD144); and over 50% of total MPs carried double antigens dominated by CD45 and CD61 positive MPs (Fig. 2*B* and Table 1). The heterotypical MP aggregates in plasma were further validated with microscopic images illustrated in Fig. 2*C–E*.

The plasma MPs used for the above characterizations were from female rats. Oestrogen has been shown to be protective in certain diseases (Brooks *et al.* 2018*b*). The gender difference in plasma MPs under STZ-induced diabetic conditions were evaluated in another 16 age-matched male and female rats 2 weeks after STZ injection. Results showed no significant gender differences in plasma MP concentration (Fig. 3, $N = 8$ per group), indicating that female protection was abolished at an early stage of STZ-induced diabetes.

The diabetic rats were induced by STZ injection. Many studies have demonstrated that the diabetic state, rather than STZ, is responsible for organ injury in STZ-induced diabetic animal models (Lee *et al.* 1974; Rasch, 1979; Evan *et al.* 1984; Churchill *et al.* 1993; Palm *et al.* 2004). To confirm that the increased plasma MPs were not the results of acute STZ toxicity in the kidneys, we evaluated the kidney function in STZ-injected rats when the plasma MPs were collected (2 weeks after STZ injection). Figure 4 shows the measurements of serum creatinine and blood urea nitrogen in normal and diabetic rats ($N =$ 7 per group). Although the measured values of serum creatinine and blood urea nitrogen in STZ rats were slightly higher than those in normal rats, they remained within the normal range. Studies have shown that values in these ranges have no detectable changes in kidney histopathology (Evan *et al.* 1984; Yu *et al.* 2010; Al-Rasheed *et al.* 2018; Xu *et al.* 2018).

Microscopic views of increased MPs in microvessels of diabetic rats

The characterization of plasma MPs provides the profile of mobile MPs in the circulation. To illustrate the increased MPs in the vasculature under diabetic conditions, we present microscopic views of MPs at the vascular walls of diabetic rats. Figure 5*A–C* shows representative confocal images of MPs adhering to a normal and a diabetic vessel. Perfusing vessels with AnnV revealed abundant MPs and some apoptotic cells at the microvessel walls of diabetic rats. The adherent leukocytes and leukocyte-MP

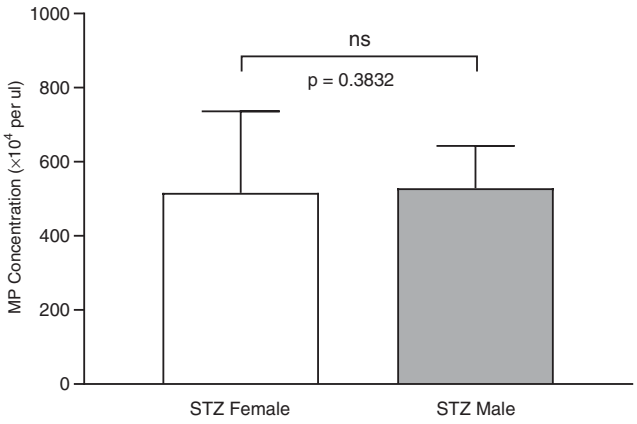

Figure 3. Comparison of gender difference in plasma microparticles (MPs) of streptozotocin (STZ)-induced diabetic rats
Flow cytometry analysis of MPs in plasma of age-matched male and female rats 2 weeks after STZ injection. Results showed no significant difference in plasma MP concentrations between STZ-injected male and female rats, indicating that female protection was abolished at an early stage of STZ-induced diabetes (non-parametric Mann-Whitney test, two-tailed). Data are presented as means ± SEM with $N = 8$ per group.

interactions on the vessel walls were shown by simultaneous staining with AnnV and CD45 antibody ($N = 5$). Such observations were absent in vessels of normal rats ($N = 4$). The fluorescence images are further confirmed by EM studies. A large number of MPs were shown at the EC surface of diabetic venules ($N = 5$), but not normal venules ($N = 6$, Fig. 5*D* and *E*), which could be newly formed EC-derived MPs or remotely transferred MPs via circulation from other regions. Figure 5*F* shows the formation of MPs from a neutrophil migrating across a diabetic venular wall, providing a microscopic evidence that the activation of WBCs contributes to the increased formation of WBC-derived MPs in diabetic rats.

Elevated MPs in diabetic plasma propagate inflammation to normal venules by mediating leukocyte adhesion and increasing endothelial cell susceptibility to inflammatory stimulus

The actions of MPs in normal and diabetic plasma on ECs were investigated in individually perfused mesenteric venules of normal rats. Each vessel was perfused with normal or diabetic rat platelet-free plasma (PFP, 50% in BSA-Ringer perfusate) for 30 min followed by AnnV perfusion for 10 min to mark the adherent MPs on the vessel walls. The confocal images shown in Fig. 6*A* were acquired after the vessel lumen AnnV was washed away with albumin-Ringer perfusate. The results showed that only the MPs in diabetic plasma, not normal plasma, rapidly adhered to the microvessel walls ($N = 3$ per group). We then examined the effects of adhered diabetic MPs on microvessel permeability and leukocyte adhesion in diabetic PFP-perfused venules. The baseline L_p and adherent leukocytes were assessed first in each vessel with BSA-Ringer perfusion. Then the changes in L_p were measured when the same vessel was perfused with either normal or diabetic PFP. The role of PFP in mediating leukocyte adhesion was examined by resuming blood flow in each perfused vessel to allow endogenous blood cells to interact with ECs that have been exposed to perfused PFP. The experimental procedures are illustrated in Fig. 6*B*. Results showed that perfusion of normal rat PFP did not cause significant changes in basal L_p and leukocyte adhesion ($N = 4$), whereas perfusion of diabetic PFP increased L_p from a mean basal value of 1.6 ± 0.2 to $11.0 \pm 1.1 \times 10^{-7}$ cm/s/cmH_2O ($N = 9$, $P = 0.001$), and the adherent leukocytes were increased from a mean value of 1.2 ± 0.2 to 15.2 ± 1.2 per 100 μm of vessel length after blood flow was resumed in PFP perfused vessels for 10 min ($N = 5$, $P < 0.001$). Removal of MPs from diabetic plasma ($N = 4$) significantly attenuated the increased L_p to $2.7 \pm 0.9 \times 10^{-7}$ cm/s/cmH_2O ($P = 0.001$), and abolished the effect of diabetic plasma on leukocyte adhesion. Figure 6*C* shows representative images of individual vessels before and after perfusion of normal and diabetic plasma, respectively. Figure 6*D* and *E* presents the results summary.

To further investigate whether exposure of a normal vessel to diabetic PFP alters the vessel susceptibility to inflammatory mediators similarly to that observed in diabetic vessels (Yuan *et al.* 2014), PAF (10 nM) was applied to four of the nine vessels that had a prior perfusion of diabetic PFP. The mean peak L_p response increased to $61.5 \pm 10.0 \times 10^{-7}$ cm/s/cmH_2O, which was significantly higher than $11.5 \pm 2.1 \times 10^{-7}$ cm/s/cmH_2O ($N = 5$), the PAF response measured in normal vessels without prior

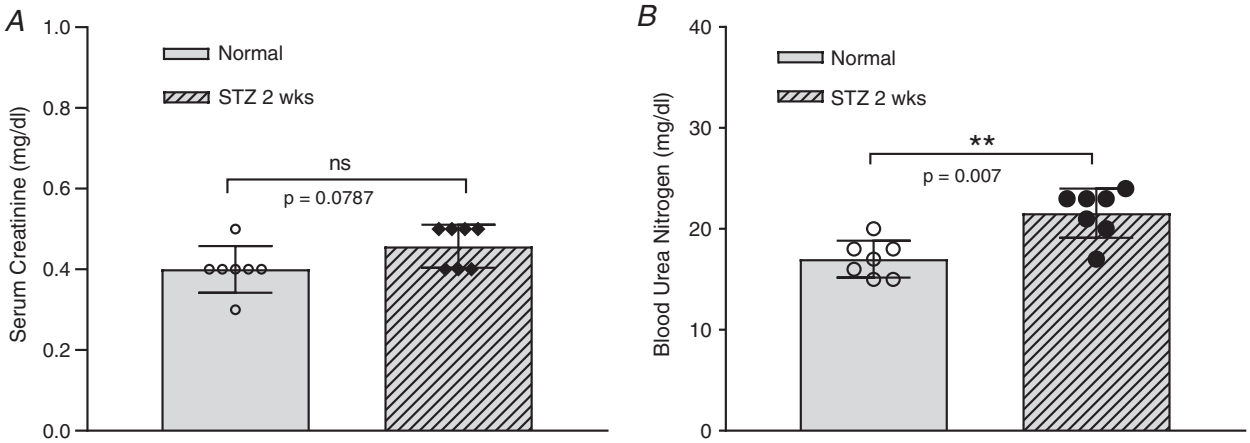

Figure 4. Kidney function evaluation of streptozotocin (STZ)-induced diabetic rats
Diabetic rats were inducted by a single intraperitoneal injection of STZ in citrate buffer (60 mg/kg body weight). Serum creatinine (*A*) and blood urea nitrogen (*B*) were measured in normal (control) and STZ-injected rats (2 weeks after STZ injection when plasma microparticles were assessed). Although the measured values of serum creatinine and blood urea nitrogen in STZ rats were slightly higher than those in normal rats, they remained within the normal range. Data are presented as individual values and the means ± SD, with $N = 7$ per group (non-parametric Mann-Whitney test, two-tailed).

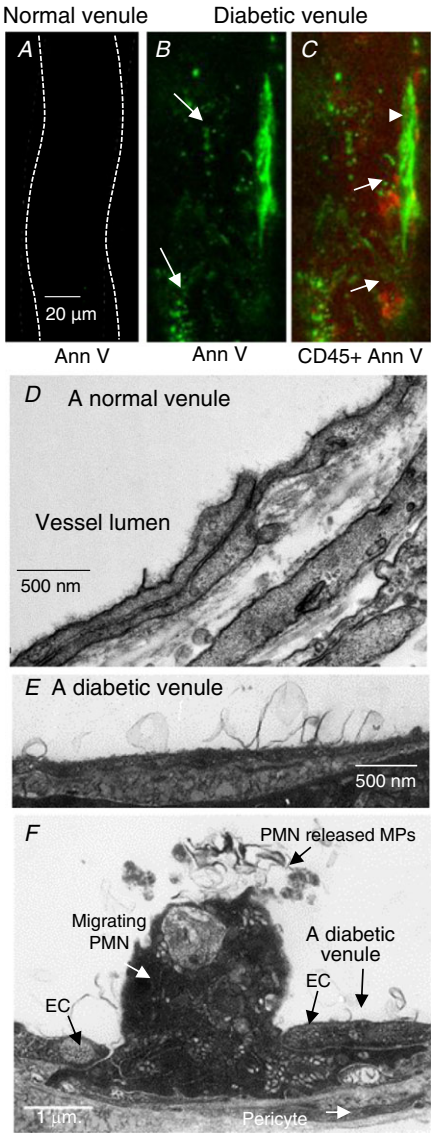

Figure 5. Microscopic illustration of microparticles (MPs) at microvessel walls of normal and diabetic rats
A–C, representative confocal images acquired after a normal and a diabetic venule were perfused with AnnV. Abundant AnnV+ (green) MPs (arrows in *B*) and some apoptotic cells (arrowhead in *C*) are detected at the diabetic vessel walls. Simultaneous staining with antibody against leukocytes, CD45 (red, arrows), illustrates the adherent leukocytes on the vessel wall. No staining was detected in vessels from normal rats (*A*). *D* and *E*, electron micrographs show the venular walls from a normal and a diabetic rat, respectively. Many MPs were observed at the EC surface of diabetic venules, but not in normal venules. *F*, micrograph showing the formation of MPs from a neutrophil (PMN) migrating across a diabetic venular wall, indicating that the activation of WBCs contributes to the increased formation of WBC-derived MPs in diabetic rats. Images are representations of studies conducted in 4–6 animals per group per approach.

diabetic PFP exposure ($P = 0.0001$), but close to the mean peak value of $62.4 \pm 7.8 \times 10^{-7}$ cm/s/cmH_2O ($N = 6$) when diabetic vessels were exposed to PAF. Figure 6*F* shows the results summary.

Increased circulating MPs disseminate inflammation in the vasculature through systemic circulation

To further investigate the causal relationship between increased plasma MPs and the inflammatory manifestations found in diabetic vessels, we conducted systemic cross-transfusion experiments between diabetic and normal rats. The changes in leukocyte adhesion and microvessel permeability were assessed after systemic transfusion of diabetic rat plasma, with and without removal of MPs, into the circulation of a normal rat. Figure 7*A* shows the vessel images acquired after plasma transfusion for 30 min and Fig. 7*B* shows L_p measurements (top) and the number of adherent leukocytes (bottom) under three different experimental conditions. When 25% of the blood volume from a normal rat was replaced by the same volume of plasma from another normal rat (control), there were no significant changes in leukocyte adhesion and microvessel L_p (left image, $N = 4$). To confirm the vessel responsiveness to inflammatory mediators, each vessel was exposed to PAF (10 nM) afterwards. All of the four vessels in the control group showed a typical PAF response (Zhu & He, 2005; Jiang *et al.* 2008), with mean L_p increased from 1.9 ± 0.4 cm/s/cmH_2O (before PAF) to a peak value of $14.0 \pm 2.4 \times 10^{-7}$ cm/s/cmH_2O. However, when diabetic plasma containing elevated MPs was transfused into a normal rat following the same procedure, the averaged adherent leukocytes were increased to 11.0 ± 2.0 per 100 μm of vessel length (middle image) and the mean L_p was $6.1 \pm 1.5 \times 10^{-7}$ cm/s/cmH_2O ($N = 6$), which was significantly higher than that of the control group ($P \leq 0.001$). We then removed MPs from diabetic plasma. When the MP-free diabetic plasma was transfused into a normal rat, leukocyte adhesion was significantly reduced to 2.0 ± 0.6 per 100 μm of vessel length, and the L_p was slightly reduced to $5.5 \pm 0.6 \times 10^{-7}$ cm/s/cmH_2O ($N = 5$). These results strongly support the hypothesis that the increased levels of MPs in diabetic plasma play important roles in mediating leukocyte adhesion and disseminating inflammation throughout the vascular system.

Externalized phosphatidylserine on diabetic MPs mediates MP interaction with endothelium and circulating leukocytes

To determine if the quantity of MPs between normal and diabetic plasma contributes to the differences of MP adhesion to endothelium, individual mesenteric venules from normal rats were perfused with MPs isolated from normal or diabetic plasma at equal concentrations

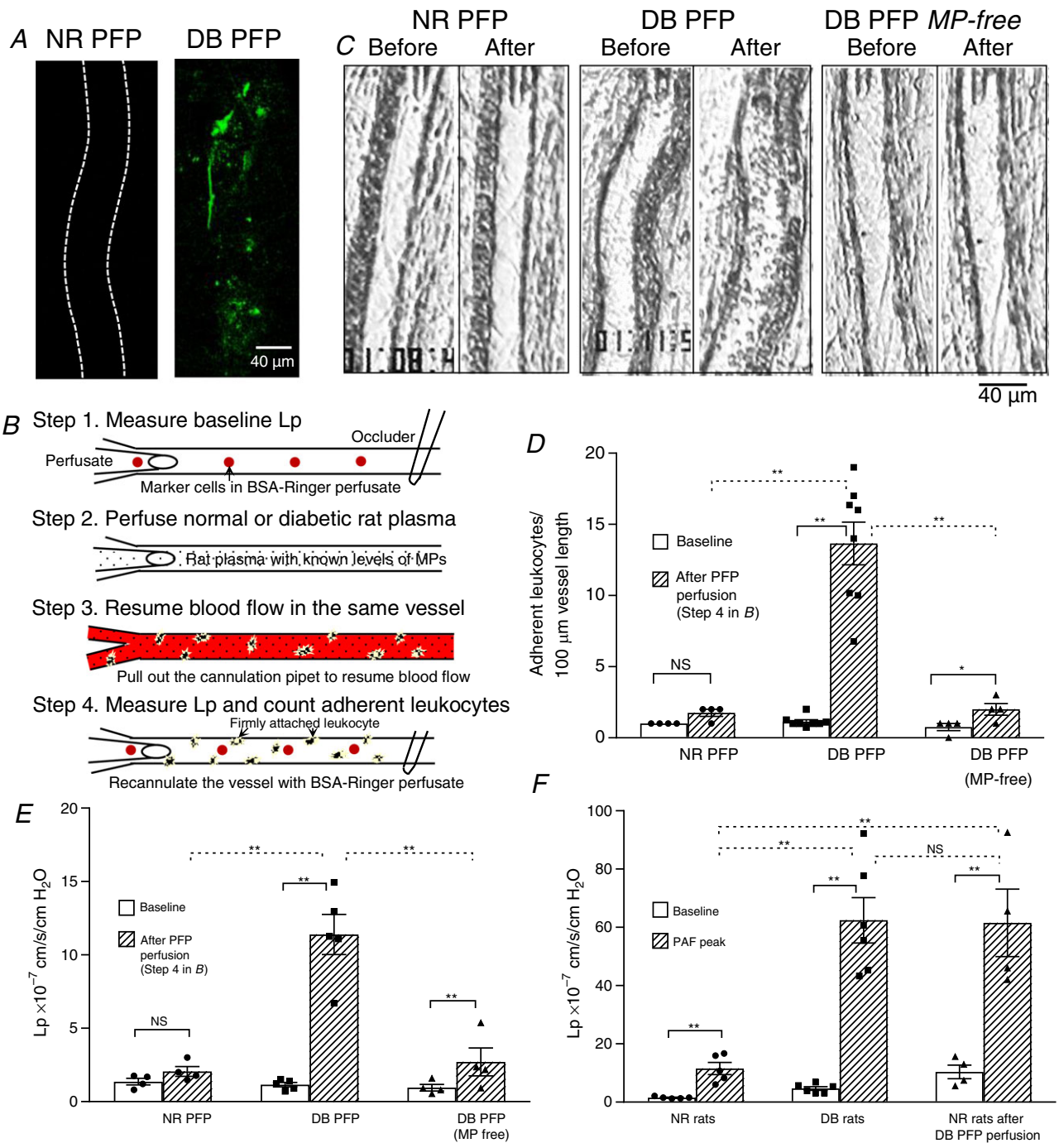

Figure 6. Increased MPs in diabetic plasma mediate leukocyte adhesion, increase microvessel permeability and alter the endothelial cell susceptibility to inflammatory stimulus
A, confocal images showing abundant adherent MPs on the wall of diabetic (DB) platelet-free plasma (PFP)-perfused vessel, but not on the normal (NR) PFP-perfused vessel. The microvessels were perfused with NR or DB PFP for 30 min followed by AnnV perfusion to mark the adherent MPs (green dots). The confocal images were acquired after lumen free AnnV was washed away with albumin-Ringer perfusate. Both images are the projection of image stacks acquired from the lower half of the microvessel ($N = 3$ per group). *B*, schematic illustration of experimental procedures for *C–F*. *C*, representative images showing individual vessels before and after perfusion of either NR PFP ($N = 4$), DB PFP ($N = 9$), or MP-free DB PFP ($N = 5$) following the procedures illustrated in *B*. *D* and *E*, summary results of DB MP-mediated leukocyte adhesion (*D*) and changes in microvessel permeability, L_p (*E*). *F*, summary results showing a direct comparison of the magnitude of PAF-induced L_p increases in vessels from NR ($N = 5$) and DB ($N = 6$) rats, and normal rat vessels with and without prior exposure to DB PFP ($N = 4$ per group). $^*P < 0.05$; ** $P \leq 0.001$; NS, $P > 0.1$.

(8600 AnnV+ MPs/μl in albumin-Ringer solution) for 30 min followed by 10 min perfusion of AnnV to mark the adherent MPs on the vessel walls. Confocal images were collected after AnnV was washed away from the vessel lumen with albumin-Ringer perfusion. Images showed that only diabetic MPs, not normal MPs, rapidly adhered to the microvessel walls ($N = 5$ per group). Pre-coating diabetic MPs with AnnV, which blocked exposed PS, prevented diabetic MP adhesion ($N = 4$), indicating that the exposed PS on the surface of diabetic MPs plays a key role in MP adhesion to endothelium. Representative images and the quantification of AnnV fluorescence intensity (FI) of the vessel walls are shown in Figure 8*A* and *C*.

We then investigated the role of exposed PS on MPs in mediating leukocyte adhesion by perfusing vessels with matched concentrations of isolated normal and diabetic MPs (8600 AnnV+ MPs/μl in albumin-Ringer solution) followed by resumed blood flow. Similar to the results with plasma perfusion, significant leukocyte adhesion only occurred in vessels perfused with diabetic MPs (15.1 ± 1.7 leukocytes/100 μm vessel length, $N = 7$), not normal MPs ($N = 4$). In another four vessels, AnnV was applied to the vessel lumen after diabetic MP perfusion to block the PS on adherent MPs before resuming blood flow. This completely blocked the diabetic MP-mediated leukocyte adhesion. Figure 8*B* & *D* shows the representative images. A summary of the results is shown in Fig. 8*E*.

We then compared the extent of the exposed PS between diabetic and normal MPs by quantifying MP binding to AnnV. Flow cytometry analysis showed that diabetic MPs exhibited significantly greater AnnV intensity than normal rat MPs ($P = 0.01$, $N = 6$ and 7, Fig. 9*A* and *C*). The average size of diabetic MPs referenced by forward scatter histograms was actually smaller than that of normal MPs (67%, $N = 5$ and 6, Fig. 9*B* and *D*). If we normalize the AnnV FI to the surface area of MPs, assuming a spherical shape, the externalized PS in diabetic MPs is 7.4-fold greater than that in normal MPs (Fig. 9*E*).

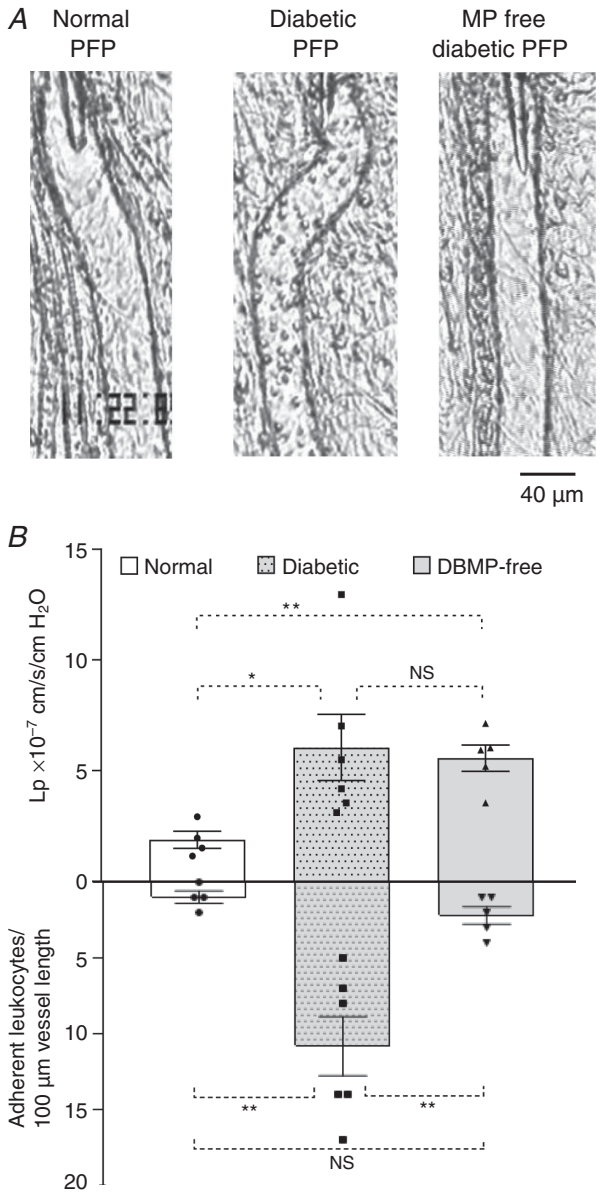

Figure 7. Increased circulating MPs disseminate inflammation through systemic circulation
A, images of representative rat venules from three groups of studies. *B*, results summary showing that transfusion of diabetic plasma into a normal rat caused increased microvessel permeability (top graph) and leukocyte adhesion (lower graph) in the recipient rat (middle image, $N = 6$), and no significant changes occurred with transfusion of plasma from a normal donor rat (left image, $N = 4$). Removal of MPs from diabetic plasma abolished its effect on leukocyte adhesion and slightly attenuated the increased permeability (right image, $N = 5$). $^*P < 0.05$; $^{**}P \leq 0.001$; NS, $P > 0.1$.

Discussion

This study provided detailed characterization of plasma MPs of diabetic animals and delineated their functional roles in intact microvessels using combined single vessel perfusion and systemic plasma transfusion approaches along with microscopic visualization and quantitative measurements of vascular permeability. The microvessel images revealed the biogenesis and manifestations of diabetes-induced MPs in the vasculature, and provided *in vivo* evidence that the elevated MPs under diabetic conditions are not merely the byproducts of activated cells, but serve as vectors and actively disseminate inflammation throughout the vascular system.

The characterization of the plasma MPs presents technical challenges due to their submicron sizes (van der Pol *et al.* 2010, 2013; Nolan & Jones, 2017). The profile of diabetes-induced circulating MPs presented here is the result of our significant effort to optimize equipment and sample preparation procedures. The plasma of diabetic rats showed a more than 100-fold increase in circulating MPs when compared to that of normal rats. Over 90%

of the increased MPs have a PS exposed surface and are mainly derived from platelets, leukocytes and endothelial cells. Importantly, our results revealed that under diabetic conditions, the majority of the increased MPs existed as aggregated units expressing multiple cell antigens. The aggregated status of plasma MPs detected by flow cytometry was validated with different microscopy approaches. With a large population of PS exposed MPs, it is not surprising that the MPs derived from different cell types interact in the circulation to form aggregate units. Individual MPs that express multiple cell markers have also been reported in an air decompression murine model (Thom *et al.* 2011). The importance of this observation is that the functional consequences of these increased MPs under diseased conditions are attributed to heterogeneous cell type-derived MPs, and are unlikely to be caused by MPs derived from a single cell source alone.

Our recent study found that microvessels of diabetic rats have abundant adherent leukocytes with moderately increased baseline permeability. However, when the vessel was exposed to an inflammatory mediator, it showed a markedly potentiated permeability increase (Yuan *et al.* 2014), which resembles the exacerbated inflammation commonly found in diabetic patients with an acute infection. Our findings indicate that certain compositions of diabetic plasma play a priming role in ECs and transform them into a pro-inflammatory phenotype with increased susceptibility to additional inflammatory stimulus. The images and micrographs in Fig. 5 provided microscopic views of venular microvessels

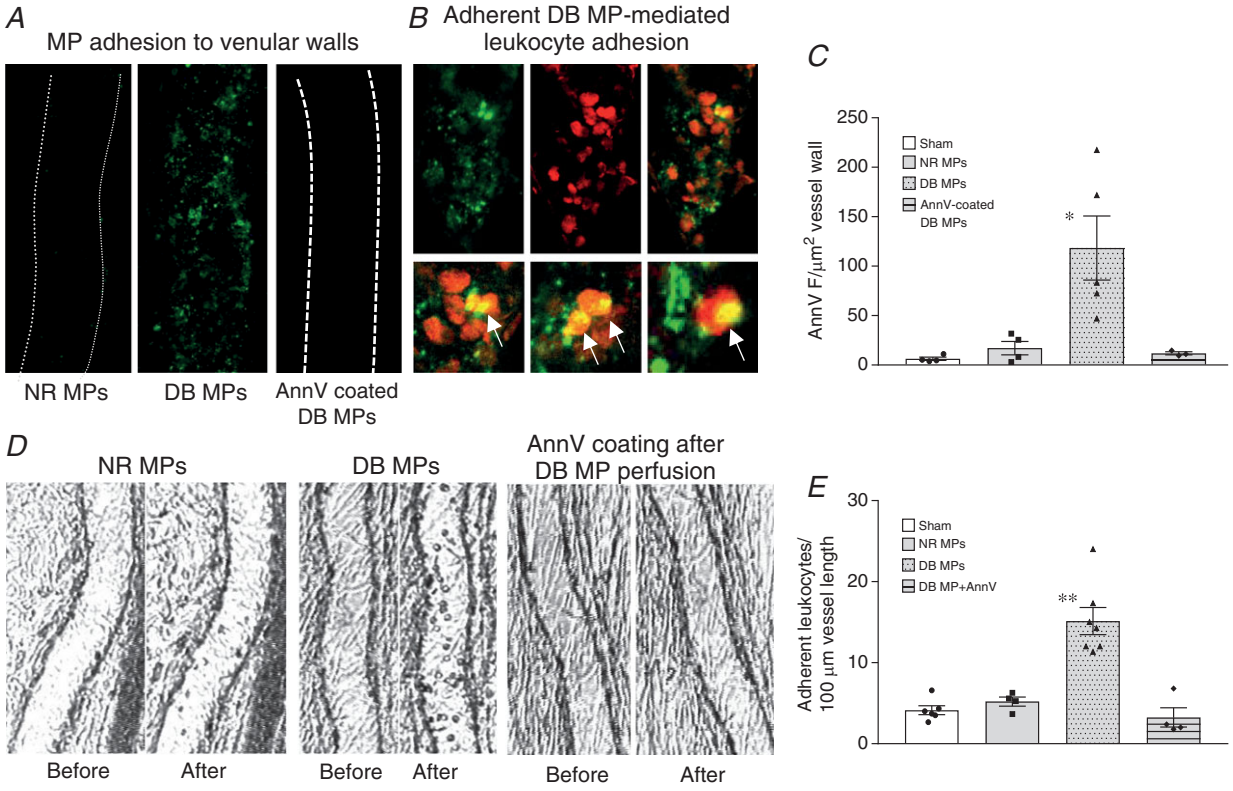

Figure 8. The externalized phosphatidylserine on diabetic microparticles (DB MPs) mediates their interactions with endothelium and circulating leukocytes
A, representative confocal images show that only DB MPs (middle), not normal (NR) MPs (left), adhered to microvessel walls (marked green by AnnV labelling), even with matched MP concentrations. Blocking surface PS by pre-coating DB MPs with AnnV prevented their adhesion (right). *B*, a representative vessel segment showing the adherent DB MP-mediated leukocyte adhesion. Adherent MPs were marked by AnnV (green, top left) and adherent MP-mediated leukocyte adhesion was labelled by Anti-CD-45 antibody (red, top middle). The top right image is the merged channel with local amplified regions shown in the lower row for details. *C*, summary of the quantification of AnnV fluorescence intensity (FI) at vessel walls as an indication of the number of adherent MPs of 4 groups ($N = 5$ for NR and DB MP group, $N = 4$ for AnnV pre-coated DB MP group and sham control). *D*, isolated MP studies show that even with equal concentrations of MPs, only perfusion of diabetic MPs ($N = 7$), not normal MPs ($N = 4$), caused a significant leukocyte adhesion (left and middle images). Blocking the PS on adherent diabetic MPs on the vessel wall by perfusing AnnV into diabetic MP-perfused vessels before resuming blood flow abolished diabetic MP-mediated leukocyte adhesion (right images, $N = 4$). *E*, results summary for experiments presented in *D* ($N = 6$ for sham control). $^{*}P < 0.05$ and $^{**}P < 0.001$ compared to the rest groups.

in diabetic rats, illustrating the adherent and/or produced MPs, attached and migrating leukocytes, and apoptotic vascular ECs in the venular walls. Our individual vessel perfusion experiments demonstrated that the exposure of normal vessels to diabetic plasma with elevated MPs quickly resulted in massive MP adhesion followed by adherent MP-mediated leukocyte adhesion. Importantly, the vascular permeability responses to PAF after diabetic plasma perfusion increased from 6- to 7-fold (normal vessel response without prior diabetic plasma perfusion) to over 30-fold of its baseline L_p. This potentiated PAF response basically replicates those observed in diabetic microvessels (Fig. 6*F*). Our results that removal of MPs from diabetic plasma abolished the leukocyte adhesion and attenuated the permeability increase differentiated the effects of MPs from other components in diabetic plasma. These observations indicate that the elevated MPs under diabetic conditions are highly adhesive. Their interactions with vascular ECs and circulating leukocytes directly contribute to the vascular vulnerability observed in diabetic patients and animals. The systemic cross-transfusion experiments with similar results to those observed in individually perfused microvessels further demonstrate the potency of elevated circulating MPs in propagation of inflammation from local regions to remote vasculatures, providing a mechanistic explanation of easily spread systemic inflammation and multi-organ microvascular dysfunction commonly found in diabetic patients. The elevated circulating MPs have also been reported to be able to interact with circulating neutrophils, resulting in neutrophil activation, further MP production, and subsequent vascular injury (Thom *et al.* 2011; Yang *et al.* 2012).

Our isolated microparticle studies allowed us to distinguish whether the quantity or quality of the MPs contributes to the functional differences observed in normal and diabetic plasma perfused vessels. Even with matched MP concentrations, only MPs isolated from diabetic plasma, not normal plasma, adhered to vascular walls, suggesting that the mechanism is based on differences in quality. Many plasma membrane adhesion molecules could be carried by MPs and potentially mediate the MP interaction with ECs and leukocytes. The externalized PS on the surface of MPs has also been recognized to be highly adhesive and procoagulant. The pro-coagulant activity of PS exposed MPs has been reported to be critical for disease associated thromboembolic complications (Campello *et al.* 2011; Yang *et al.* 2016; Zhao *et al.* 2016, 2017; Ridger *et al.* 2017). In contrast, the adhesive property of PS in MP-mediated vascular inflammation has not been well defined. Unexpectedly, pre-coating diabetic MPs with AnnV completely blocked

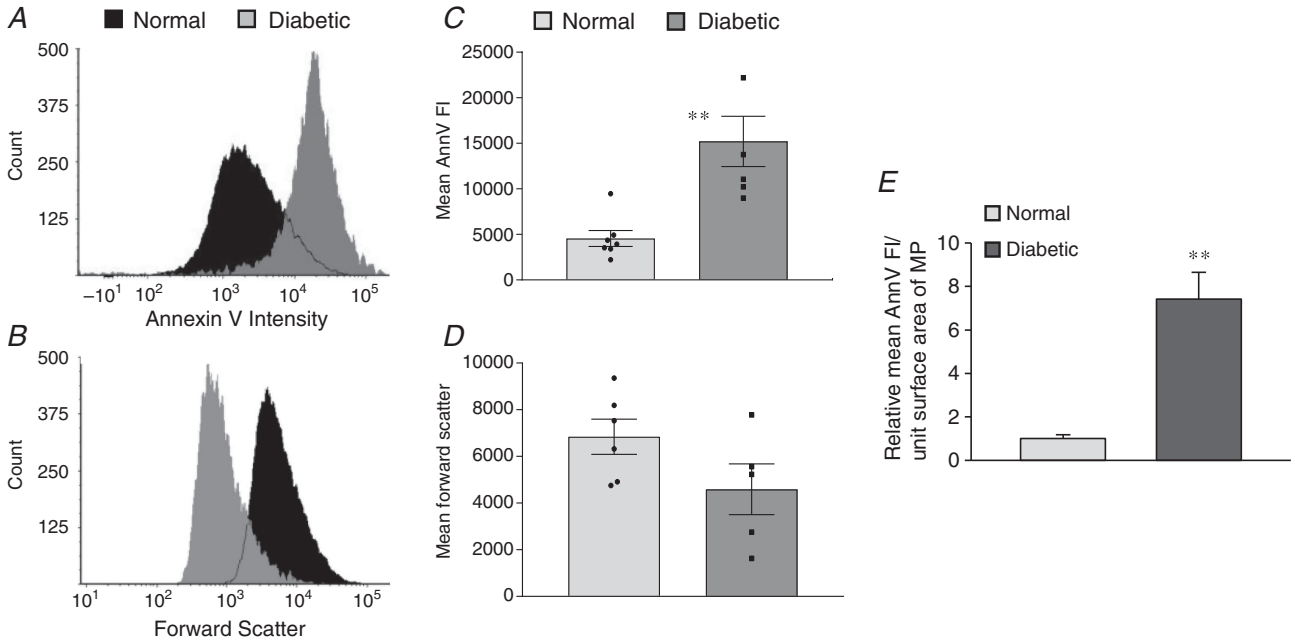

Figure 9. Flow cytometry analysis showing microparticles (MPs) isolated from diabetic rat plasma to be smaller in size and have greater phosphatidylserine exposed surface area compared to MPs isolated from normal rat plasma
A and *B*, representative histograms demonstrating the differences in the AnnV fluorescent intensity (FI) and the size distribution (forward scatter) of isolated MPs from diabetic and normal plasma at equal concentration. *C* and *D*, summary results showing the mean AnnV FI ($N = 6$ and 7 per group) and forward scatter data ($N = 5$ and 6 per group) of normal and diabetic MPs. *E*, comparison of the mean AnnV FI between diabetic and normal MPs with normalized surface area of MPs (derived from data in *C* and *D*). $^{**}P \leq 0.01$.

diabetic MP interactions with both ECs and circulating leukocytes, indicating that the externalized PS on the MP surface was the main contributing factor to the adhesive properties of diabetic MPs. Additionally, the PS-mediated adhesion rapidly occurred in normal vessels, suggesting there is no need for the activation of counter ligands on endothelium. Although the percentage of positive MP binding to AnnV in diabetic plasma is significantly higher than in normal plasma (92% *vs.* 78%), we consider the extent of the PS exposure on the MP surface to be the key factor. The density of AnnV binding to membrane is reported to be primarily affected by the PS content and calcium, and less by intrinsic affinity of the binding site (Tait & Gibson, 1992). Our results that an average of 7 times higher AnnV fluorescence intensity per unit surface area in diabetic MPs than normal MPs indicate that diabetic MPs have much larger PS exposed surface area than normal MPs. This significantly higher AnnV binding in diabetic MPs together with the observation that pre-coating diabetic MPs with AnnV completely abolished diabetic MP-mediated adhesion support that the largely exposed PS surface area in MPs from diabetic rats plays a critical role in mediating MP/endothelium and MP/leukocyte interaction and subsequently alter vascular susceptibility to inflammation.

Most of the data presented here were derived from female rats. Although oestrogen has been shown to be protective in certain diseases (Brooks *et al.* 2018*b*) and beneficial in human health in general, reduced or abolished female protection has been reported in diabetic patients (McCollum *et al.* 2005; Kalyani *et al.* 2014), diabetic rats (He P, Xia X, LaPenna KB & Zhang Y; in press), and in animals with preexisting metabolic diseases (Brooks *et al.* 2018*a*). In this study, we also found no significant differences in plasma MP concentrations between STZ-induced male and female diabetic rats (Fig. 3), which is consistent with our permeability studies in diabetic rats and other reports, indicating oestrogen did not exert sufficient anti-inflammatory and antioxidant effects under diabetic conditions. The mechanisms involved in the lost female protection in diabetes and metabolic diseases remain to be identified. This study focused on the functional roles of diabetes-induced circulating MPs in propagating inflammation in microvessels. The vascular permeability and phenotypic changes of female diabetic rats have been well characterized in our previous studies (Yuan *et al.* 2014), therefore, female rats were used in most of the studies.

An increase in circulating MPs has been reported in many cardiovascular diseases (Agouni *et al.* 2008; Berezin & Kremzer, 2015; Berezin *et al.* 2015; Badimon *et al.* 2017; Ridger *et al.* 2017). The MPs we studied were derived from STZ-induced diabetic rats. Although STZ is a cytotoxic agent, due to its short biological half-life and its preferential uptake by pancreatic β cells, any off-target toxicity has been demonstrated to be minimal, short-lived, and reversible with proper dosage. There have been many studies using variable approaches to differentiate the effects of STZ from STZ-induced hyperglycaemia on kidney and other organ functions (Lee *et al.* 1974; Rasch, 1979; Evan *et al.* 1984; Churchill *et al.* 1993; Palm *et al.* 2004), which all concluded that the diabetic state, rather than STZ, is responsible for organ injury. Those studies provided solid characterization and validation for the use of this model. Currently STZ-induced diabetic rodent models are widely accepted tools for investigating the mechanisms of diabetes-associated organ complications and potential therapeutics interventions (Deeds *et al.* 2011; Furman, 2015). Our kidney function evaluation in rats 2 weeks after STZ-injection (Fig. 4) also does not support an acute STZ toxicity-induced kidney dysfunction (Evan *et al.* 1984; Yu *et al.* 2010; Al-Rasheed *et al.* 2018; Xu *et al.* 2018). Based on our and others' experimental evidence, we conclude that the diabetic state is responsible for the large increase in plasma MPs in STZ-induced diabetic rats.

In summary, using unique experimental approaches, this study presents microscopic visualization of diabetes-initiated MP production and its manifestations in the vasculature. MPs produced under different environments by different cell types play distinct roles in vascular function, both beneficial and detrimental. This study also reveals the actions of diabetes-induced elevated circulating MPs in the initiation and propagation of inflammation in the vasculature and provides mechanistic insight into the pathogenesis of multi-organ vascular inflammation that commonly occurs in diabetic patients. We also observed that a large number of adherent MPs endocytosed into ECs lining the microvessel walls. The contents of diabetic MPs delivered into ECs and the long-term effect of MP-delivered components to ECs on diabetes-associated vascular complications is the focus of future studies.

References

Agouni A, Lagrue-Lak-Hal AH, Ducluzeau PH, Mostefai HA, Draunet-Busson C, Leftheriotis G, Heymes C, Martinez MC & Andriantsitohaina R (2008). Endothelial dysfunction caused by circulating microparticles from patients with metabolic syndrome. *Am J Pathol* **173**, 1210–1219.

Al-Rasheed NM, Al-Rasheed NM, Bassiouni YA, Hasan IH, Al-Amin MA, Al-Ajmi HN & Mahmoud AM (2018). Simvastatin ameliorates diabetic nephropathy by attenuating oxidative stress and apoptosis in a rat model of streptozotocin-induced type 1 diabetes. *Biomed Pharmacother* **105**, 290–298.

Badimon L, Suades R, Arderiu G, Pena E, Chiva-Blanch G & Padro T (2017). Microvesicles in atherosclerosis and angiogenesis: from bench to bedside and reverse. *Front Cardiovasc Med* **4**, 77.

Berezin AE & Kremzer AA (2015). Impaired phenotype of circulating endothelial microparticles in chronic heart failure patients: Relevance to body mass index. *Diabetes Metab Syndr* **9**, 230–236.

Berezin AE, Kremzer AA, Samura TA, Berezina TA & Kruzliak P (2015). Impaired immune phenotype of circulating endothelial-derived microparticles in patients with metabolic syndrome and diabetes mellitus. *J Endocrinol Invest* **38**, 865–874.

Boilard E, Nigrovic PA, Larabee K, Watts GF, Coblyn JS, Weinblatt ME, Massarotti EM, Remold-O'Donnell E, Farndale RW, Ware J & Lee DM (2010). Platelets amplify inflammation in arthritis via collagen-dependent microparticle production. *Science* **327**, 580–583.

Brooks SD, Hileman SM, Chantler PD, Milde SA, Lemaster KA, Frisbee SJ, Shoemaker JK, Jackson DN & Frisbee JC (2018*a*). Protection from chronic stress- and depressive symptom-induced vascular endothelial dysfunction in female rats is abolished by preexisting metabolic disease. *Am J Physiol Heart Circ Physiol* **314**, H1085–H1097.

Brooks SD, Hileman SM, Chantler PD, Milde SA, Lemaster KA, Frisbee SJ, Shoemaker JK, Jackson DN & Frisbee JC (2018*b*). Protection from vascular dysfunction in female rats with chronic stress and depressive symptoms. *Am J Physiol Heart Circ Physiol* **314**, H1070–H1084.

Burger D, Turner M, Xiao F, Munkonda MN, Akbari S & Burns KD (2017). High glucose increases the formation and pro-oxidative activity of endothelial microparticles. *Diabetologia* **60**, 1791–1800.

Campello E, Spiezia L, Radu CM, Bulato C, Castelli M, Gavasso S & Simioni P (2011). Endothelial, platelet, and tissue factor-bearing microparticles in cancer patients with and without venous thromboembolism. *Thromb Res* **127**, 473–477.

Churchill P, Churchill M, Bidani A & Dunbar J Jr (1993). Streptozotocin-induced renal hemodynamic changes in isogenic Lewis rats: a kidney transplant study. *Am J Physiol* **264**, F100–F105.

Deeds MC, Anderson JM, Armstrong AS, Gastineau DA, Hiddinga HJ, Jahangir A, Eberhardt NL & Kudva YC (2011). Single dose streptozotocin-induced diabetes: considerations for study design in islet transplantation models. *Lab Anim* **45**, 131–140.

Dey-Hazra E, Hertel B, Kirsch T, Woywodt A, Lovric S, Haller H, Haubitz M & Erdbruegger U (2010). Detection of circulating microparticles by flow cytometry: influence of centrifugation, filtration of buffer, and freezing. *Vasc Health Risk Manag* **6**, 1125–1133.

Evan AP, Mong SA, Gattone VH, Connors BA, Aronoff GR & Luft FC (1984). The effect of streptozotocin and streptozotocin-induced diabetes on the kidney. *Ren Physiol* **7**, 78–89.

Furman BL (2015). Streptozotocin-induced diabetic models in mice and rats. *Curr Protoc Pharmacol* **70**, 5.47.1–5.47.20.

Grundy D (2015). Principles and standards for reporting animal experiments in *The Journal of Physiology* and *Experimental Physiology*. *J Physiol* **593**, 2547–2549.

Gyorgy B, Modos K, Pallinger E, Paloczi K, Pasztoi M, Misjak P, Deli MA, Sipos A, Szalai A, Voszka I, Polgar A, Toth K, Csete M, Nagy G, Gay S, Falus A, Kittel A & Buzas EI (2011). Detection and isolation of cell-derived microparticles are compromised by protein complexes resulting from shared biophysical parameters. *Blood* **117**, e39–48.

He P, Zhang H, Zhu L, Jiang Y & Zhou X (2006). Leukocyte-platelet aggregate adhesion and vascular permeability in intact microvessels: role of activated endothelial cells. *Am J Physiol Heart Circ Physiol* **291**, H591–H599.

He P, Zhang X & Curry FE (1996). Ca^{2+} entry through conductive pathway modulates receptor-mediated increase in microvessel permeability. *Am J Physiol* **271**, H2377–H2387.

Helal O, Defoort C, Robert S, Marin C, Lesavre N, Lopez-Miranda J, Riserus U, Basu S, Lovegrove J, McMonagle J, Roche HM, Dignat-George F & Lairon D (2010). Increased levels of microparticles originating from endothelial cells, platelets and erythrocytes in subjects with metabolic syndrome: Relationship with oxidative stress. *Nutr Metab Cardiovasc Dis* **21**, 665–671.

Hosseinzadeh S, Noroozian M, Mortaz E & Mousavizadeh K (2018). Plasma microparticles in Alzheimer's disease: The role of vascular dysfunction. *Metab Brain Dis* **33**, 293–299.

Jiang Y, Wen K, Zhou X, Schwegler-Berry D, Castranova V & He P (2008). Three-dimensional localization and quantification of PAF-induced gap formation in intact venular microvessels. *Am J Physiol Heart Circ Physiol* **295**, H898–H906.

Jung C, Shemyakin A, Bohm F & Pernow J (2009). Endothelial microparticles in patients with insulin resistance. *Diabetes Metab* **35**, 71–73.

Kalyani RR, Lazo M, Ouyang P, Turkbey E, Chevalier K, Brancati F, Becker D & Vaidya D (2014). Sex differences in diabetes and risk of incident coronary artery disease in healthy young and middle-aged adults. *Diabetes Care* **37**, 830–838.

La Marca V & Fierabracci A (2017). Insights into the diagnostic potential of extracellular vesicles and their miRNA signature from liquid biopsy as early biomarkers of diabetic micro/macrovascular complications. *Int J Mol Sci* **18**, E1974.

Lee CS, Mauer SM, Brown DM, Sutherland DE, Michael AF & Najarian JS (1974). Renal transplantation in diabetes mellitus in rats. *J Exp Med* **139**, 793–800.

Leroyer AS, Rautou PE, Silvestre JS, Castier Y, Leseche G, Devue C, Duriez M, Brandes RP, Lutgens E, Tedgui A & Boulanger CM (2008*a*). CD40 ligand+ microparticles from human atherosclerotic plaques stimulate endothelial proliferation and angiogenesis a potential mechanism for intraplaque neovascularization. *J Am Coll Cardiol* **52**, 1302–1311.

Leroyer AS, Tedgui A & Boulanger CM (2008*b*). Microparticles and type 2 diabetes. *Diabetes Metab* **34** (Suppl. 1), S27–32.

McCollum M, Hansen LS, Lu L & Sullivan PW (2005). Gender differences in diabetes mellitus and effects on self-care activity. *Gend Med* **2**, 246–254.

Mastronardi ML, Mostefai HA, Meziani F, Martinez MC, Asfar P & Andriantsitohaina R (2011). Circulating microparticles from septic shock patients exert differential tissue expression of enzymes related to inflammation and oxidative stress. *Crit Care Med* **39**, 1739–1748.

Meziani F, Delabranche X, Asfar P & Toti F (2010). Bench-to-bedside review: circulating microparticles–a new player in sepsis? *Crit Care* **14**, 236.

Michalska-Jakubus M, Kowal-Bielecka O, Smith V, Cutolo M & Krasowska D (2017). Plasma endothelial microparticles reflect the extent of capillaroscopic alterations and correlate with the severity of skin involvement in systemic sclerosis. *Microvasc Res* **110**, 24–31.

Nolan JP & Jones JC (2017). Detection of platelet vesicles by flow cytometry. *Platelets* **28**, 256–262.

Nomura S, Ozaki Y & Ikeda Y (2008). Function and role of microparticles in various clinical settings. *Thromb Res* **123**, 8–23.

Orozco AF & Lewis DE (2010). Flow cytometric analysis of circulating microparticles in plasma. *Cytometry A* **77**, 502–514.

Palm F, Ortsater H, Hansell P, Liss P & Carlsson PO (2004). Differentiating between effects of streptozotocin per se and subsequent hyperglycemia on renal function and metabolism in the streptozotocin-diabetic rat model. *Diabetes Metab Res Rev* **20**, 452–459.

Pasquier J, Thomas B, Hoarau-Vechot J, Odeh T, Robay A, Chidiac O, Dargham SR, Turjoman R, Halama A, Fakhro K, Menzies R, Jayyousi A, Zirie M, Al Suwaidi J, Rafii A, Malik RA, Talal T & Abi Khalil C (2017). Circulating microparticles in acute diabetic Charcot foot exhibit a high content of inflammatory cytokines, and support monocyte-to-osteoclast cell induction. *Sci Rep* **7**, 16450.

Puddu P, Puddu GM, Cravero E, Muscari S & Muscari A (2010). The involvement of circulating microparticles in inflammation, coagulation and cardiovascular diseases. *Can J Cardiol* **26**, 140–145.

Ramstrom S (2005). Clotting time analysis of citrated blood samples is strongly affected by the tube used for blood sampling. *Blood Coagul Fibrinolysis* **16**, 447–452.

Rasch R (1979). Prevention of diabetic glomerulopathy in streptozotocin diabetic rats by insulin treatment. Kidney size and glomerular volume. *Diabetologia* **16**, 125–128.

Ridger VC, Boulanger CM, Angelillo-Scherrer A, Badimon L, Blanc-Brude O, Bochaton-Piallat ML, Boilard E, Buzas EI, Caporali A, Dignat-George F, Evans PC, Lacroix R, Lutgens E, Ketelhuth DFJ, Nieuwland R, Toti F, Tunon J, Weber C & Hoefer IE (2017). Microvesicles in vascular homeostasis and diseases. Position Paper of the European Society of Cardiology (ESC) Working Group on Atherosclerosis and Vascular Biology. *Thromb Haemost* **117**, 1296–1316.

Tait JF & Gibson D (1992). Phospholipid binding of annexin V: effects of calcium and membrane phosphatidylserine content. *Arch Biochem Biophys* **298**, 187–191.

Thom SR, Yang M, Bhopale VM, Huang S & Milovanova TN (2011). Microparticles initiate decompression-induced neutrophil activation and subsequent vascular injuries. *J Appl Physiol (1985)* **110**, 340–351.

Tramontano AF, Lyubarova R, Tsiakos J, Palaia T, Deleon JR & Ragolia L (2010). Circulating endothelial microparticles in diabetes mellitus. *Mediators Inflamm* **2010**, 250476.

Trummer A, De Rop C, Tiede A, Ganser A & Eisert R (2008). Isotype controls in phenotyping and quantification of microparticles: a major source of error and how to evade it. *Thromb Res* **122**, 691–700.

van der Pol E, Coumans F, Varga Z, Krumrey M & Nieuwland R (2013). Innovation in detection of microparticles and exosomes. *J Thromb Haemost* **11** (Suppl. 1), 36–45.

van der Pol E, Hoekstra AG, Sturk A, Otto C, van Leeuwen TG & Nieuwland R (2010). Optical and non-optical methods for detection and characterization of microparticles and exosomes. *J Thromb Haemost* **8**, 2596–2607.

van Ierssel SH, Van Craenenbroeck EM, Conraads VM, Van Tendeloo VF, Vrints CJ, Jorens PG & Hoymans VY (2010). Flow cytometric detection of endothelial microparticles (EMP): effects of centrifugation and storage alter with the phenotype studied. *Thromb Res* **125**, 332–339.

Xu HL, Wang XT, Cheng Y, Zhao JG, Zhou YJ, Yang JJ & Qi MY (2018). Ursolic acid improves diabetic nephropathy via suppression of oxidative stress and inflammation in streptozotocin-induced rats. *Biomed Pharmacother* **105**, 915–921.

Yang C, Ma R, Jiang T, Cao M, Zhao L, Bi Y, Kou J, Shi J & Zou X (2016). Contributions of phosphatidylserine-positive platelets and leukocytes and microparticles to hypercoagulable state in gastric cancer patients. *Tumour Biol* **37**, 7881–7891.

Yang M, Milovanova TN, Bogush M, Uzun G, Bhopale VM & Thom SR (2012). Microparticle enlargement and altered surface proteins after air decompression are associated with inflammatory vascular injuries. *J Appl Physiol (1985)* **112**, 204–211.

Yu Y, Jin H, Holder D, Ozer JS, Villarreal S, Shughrue P, Shi S, Figueroa DJ, Clouse H, Su M, Muniappa N, Troth SP, Bailey W, Seng J, Aslamkhan AG, Thudium D, Sistare FD & Gerhold DL (2010). Urinary biomarkers trefoil factor 3 and albumin enable early detection of kidney tubular injury. *Nat Biotechnol* **28**, 470–477.

Yuan D, Xu S & He P (2014). Enhanced permeability responses to inflammation in streptozotocin-induced diabetic rat venules: Rho-mediated alterations of actin cytoskeleton and VE-cadherin. *Am J Physiol Heart Circ Physiol* **307**, H44–H53.

Yun JW, Xiao A, Tsunoda I, Minagar A & Alexander JS (2016). From trash to treasure: The untapped potential of endothelial microparticles in neurovascular diseases. *Pathophysiology* **23**, 265–274.

Zhao L, Bi Y, Kou J, Shi J & Piao D (2016). Phosphatidylserine exposing-platelets and microparticles promote procoagulant activity in colon cancer patients. *J Exp Clin Cancer Res* **35**, 54.

Zhao L, Wu X, Si Y, Yao Z, Dong Z, Novakovic VA, Guo L, Tong D, Chen H, Bi Y, Kou J, Shi H, Tian Y, Hu S, Zhou J & Shi J (2017). Increased blood cell phosphatidylserine exposure and circulating microparticles contribute to procoagulant activity after carotid artery stenting. *J Neurosurg* **127**, 1041–1054.

Zhu L & He P (2005). Platelet-activating factor increases endothelial $[Ca^{2+}]_i$ and NO production in individually perfused intact microvessels. *Am J Physiol Heart Circ Physiol* **288**, H2869–H2877.

Additional information

Competing interests

The authors declare no competing financial interests.

Author contributions

Q.F., C.J.S., S.X., D.Y., X.X., G.G, H.S. and L.X. performed the research. Q.F., C.J.S., S.X., D.Y., X.X., G.G, H.S. L.X., K.B, L., K.B. and P.H. analysed data and made the figures. Q.F., C.J.S., S.X., D.Y. K.B. N.S. T.S. and P.H. designed the research, and Q.F., C.J.S. and P.H. wrote All authors have approved the final version of the manuscript and agree to be accountable for all aspects of the work. All persons designated as authors qualify for authorship, and all those who qualify for authorship are listed.the paper.

Funding

This work was supported by the National Institutes of Health Grants DK097391, HL130363, HL56237, F32HL114376, GM103488, and S10 OD016165.

Acknowledgments

The authors thank Ms Mi Zhou for her help in some of the experiments.